LAWRENCE
LIVERMORE
NATIONAL
LABORATORY

LLNL-CONF-563592

Model-based corrections to observed back azimuth and slowness observations from a dipping Mohorovicic discontinuity

M. P. Flanagan, S. C. Myers, N. A. Simmons

July 6, 2012

Monitoring Research Review
Albuquerque, NM, United States
September 18, 2012 through September 20, 2012

Disclaimer

MODEL-BASED CORRECTIONS TO OBSERVED BACK AZIMUTH AND SLOWNESS OBSERVATIONS FROM A DIPPING MOHOROVICIC DISCONTINUITY

Megan P. Flanagan, Stephen C. Myers, Nathan A. Simmons

Lawrence Livermore National Laboratory

Sponsored by the National Nuclear Security Administration

DE-AC52-07NA27344/LL12-SignalAnalysis-NDD02

ABSTRACT

Back azimuth and slowness anomalies observed at seismic arrays can be used to constrain local and distant structural and propagation effects in the Earth. Observations of large systematic deviations in both azimuth and slowness measured for several *P* phases (*i.e., Pg, Pn, P, PKP*) recorded at several IMS arrays show a characteristic sinusoidal pattern when plotted as a function of theoretical back azimuth. These deviations are often interpreted as the affect of the wavefield being systematically bent by refraction from a dipping velocity structure beneath the array, most likely a dipping Moho.

We develop a model-based technique that simultaneously fits back azimuth and slowness observations with a ray-based prediction that incorporates a dipping layer defined by its strike and dip. Because the azimuth and slowness deviations both vary as a function of true azimuth, fitting both residuals jointly will give a more consistent calibration for the array. The technique is used to fit over 9900 observations at CMAR from a global distribution of well-located seismic events.

Under the assumption that the dipping layer is the Moho with mantle velocity 8.04 km/sec and crustal velocity 6.2 km/sec, we estimate that Moho strike and dip under the CMAR array are 192.6° and 18.3°, respectively. When the trend of the Moho is removed from the back azimuth and slowness residuals, both the sinuous trend and variations with predicted slowness are mitigated. While a dipping interface model does not account for all of the discrepancy between observed and predicted back azimuth and slowness anomalies, and additional calibration whether empirical or model based should be pursued, this technique is a good first step in the calibration procedure for arrays exhibiting sinusoidal residual trends.

OBJECTIVES

The goal of this project is test the robustness of a ray-based prediction of azimuth and slowness anomalies to fit a dipping Moho geometry beneath an array. To date the modeling of such anomalies has been simplified to removing a sinusoidal-fit function from the back azimuth and slowness residuals separately. This approach does not properly account for the effect of variable slowness at a given back azimuth. Here we present a more complete model approach that simultaneously fits back azimuth and slowness observations with a ray-based prediction that incorporates a dipping Moho. Because the azimuth and slowness deviations both vary as a function of true azimuth, fitting both residuals jointly will give a more consistent calibration for the array.

RESEARCH ACCOMPLISHED

Seismic array data provide an advantage over single station data for monitoring purposes because they allow for the additional measurement of the vector velocity of an incident wave front. Specifically, the back azimuth and slowness may be determined as the seismic wavefronts sweep across the array of sensors. The back azimuth and slowness parameters are commonly used to distinguish between different seismic phases, associate arrivals to an event, and can even provide needed constraints on event location when an event is recorded at just one or two stations. Since their inception, seismic arrays have been used for both monitoring as well as numerous studies of Earth structure (see Rost and Thomas (2002) for an excellent review). However, to use arrays effectively they need to be calibrated to account for local structural effects (*e.g.,* Ringdal and Husebye, 1982; Ram and Yadav, 1984; Koch and Kradolfer, 1997; Tibuleac and Herrin, 2001; Bondar *et al*. 1999; Lindquist *et al*., 2007; Tibuleac and Stoujkova, 2009).

For Earth models with spherically symmetric velocity structure, the great-circle path from the event to the station is used to predict back azimuth, and theoretical ray parameter is used to predict slowness. Empirically, back azimuth and slowness measurements are often observed to deviate significantly from theoretical predictions, and most notably they can show a sinusoidal azimuthal dependence. Such a pattern suggests that the ray paths have been systematically bent by refraction from a dipping velocity structure beneath the array, and the Moho is a likely candidate (Figure 1). The functional relationship between the Moho strike ϕ and dip δ angles and the sinusoidal pattern of back azimuth and slowness residuals was derived by Niazi (1966) and subsequently used in several array calibration studies (*e.g.*, Otsuka, 1966a, 1966b; Greenfield and Sheppard, 1969; Havskov and Kanesewich, 1978; Koch and Kraundoffer, 1997; Tibuleac and Herrin, 1997; Schweitzer, 2001; Lindquist et al., 2007; Tibuleac and Stroujkova, 2009).

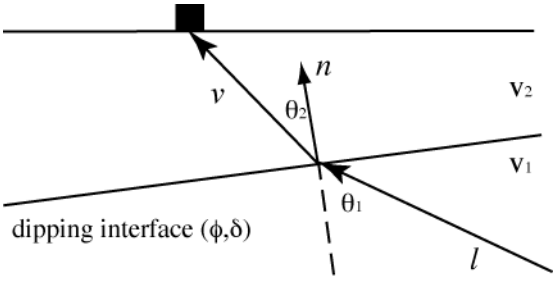

Figure 1. Geometry of the incident and refracted wavefronts with respect to a dipping interface with a specified orientation (defined by ϕ , δ). Note that the illustration is simplified to 2 dimensions, whereas the actual problem is 3-D. *l* is the directional vector of the incident beam (determined by theoretical back azimuth and slowness), *v* is the directional vector of the refracted beam, *n* is the normal vector to the dipping-Moho plane (using ϕ and δ), θ_1 is the angle of incidence, and θ_2 is the angle of refraction. We use the iasp91 *P*-wave velocities below and above the Moho, 8.04 and 6.2 km/sec respectively, for v_1 and v_2.

The discrepancies (hereafter called errors) of back azimuth and slowness can be attributed to deviations in the assumption of spherically symmetric velocity structure (model error) and measurement error. In this paper we address model error, even though measurement error is also significant. Studies based on the approach of Niazi (1966) address back azimuth and slowness model errors. For array stations with uncommonly large errors, back azimuth and slowness errors often exhibit a discernable trend when plotted as a function of theoretical back azimuth. Empirical approaches may correct for these trends if the calibration data set provides outstanding geographic coverage with minimal measurement error. However, a model-based approach may better exploit the data trend by allowing trend extrapolation for data sets with limited geographic coverage. Using a model-based first step in the calibration procedure will also improve subsequent empirical calibration because back azimuth and slowness residuals (following a model-based correction) will better adhere to the zero-mean assumption that is implicit in empirical calibration methods such as kriging.

To date the modeling has been simplified to removing a sinusoidal-fit function from the back azimuth and slowness residuals. This approach does not properly account for the effect of variable slowness at a given back azimuth. Here we present a more complete model approach to a dipping layer correction that simultaneously fits back azimuth and slowness observations with a ray-based prediction that incorporates a dipping layer defined by it's strike and dip. In this method the free parameters would be the strike ϕ and dip δ angles of the Moho plane in contrast to the phase and amplitude of cosine waves that are fit to back azimuth and slowness residuals separately. Because the azimuth and slowness deviations both vary as a function of true azimuth, fitting both residuals jointly will give a more consistent calibration.

We examine the effect of a dipping Moho discontinuity on the angle of incidence and the observed azimuth of a seismic wave, and what follows is an overview of the geometry and derivation of the equations governing the azimuthal dependence of both observed azimuth and slowness parameters, some examples of the ray-based forward predictions, and finally some examples of fitting data.

Azimuth and Slowness Measurements

We use back azimuth and slowness measurements made from *P* phases (*i.e., Pg, Pn, P, PKP*) recorded at several IMS arrays between the years 1995 and 2009. These measurements are provided by the USNDC and are produced from well-located events with epicenter error of 25 km or less (GT25) and $m_b > 4.5$. The back azimuth and slowness are estimated using a standard frequency-wavenumber algorithm (*e.g.*, Capon, 1969; Kvaerna and Doornbos, 1986). We include only those measurements having uncertainties of less than 15° for back azimuth and 1.5 sec/° for slowness, and we further restrict the slowness to be less than 13.5 sec/° as such horizontally travelling waves with high slowness cause instabilities in the optimization code. The global distribution of events provides good back-azimuthal coverage at several arrays allowing us to discern patterns in the azimuth and slowness residuals.

The back azimuth and slowness measurements are next compared with theoretical predictions made using the **iasp91** velocity model and residuals are formed. Examples of these residuals are shown in Figure 2 for the CMAR (Chiang Mai, Thailand) and ILAR (Eilelson, Alaska) arrays. Both the back azimuth and slowness residuals show the characteristic sinusoidal shape indicative of a dipping layer beneath the array. Note the effect of slowness (incoming ray inclination) on the magnitude of the azimuth deflection. The effect of the dipping interface is strongest for rays that approach the interface with a small slowness (*i.e.,* at a steep angle).

We observe this pattern in the residual distribution at a number of IMS arrays and report results here for only CMAR and ILAR as there are calibration studies for both of these arrays, by Tibuleac and Stroujkova (2009) and Lindquist *et al*. (2007), which use the Niazi (1966) approach to determine Moho dip and strike and thus provide a direct comparison with our results.

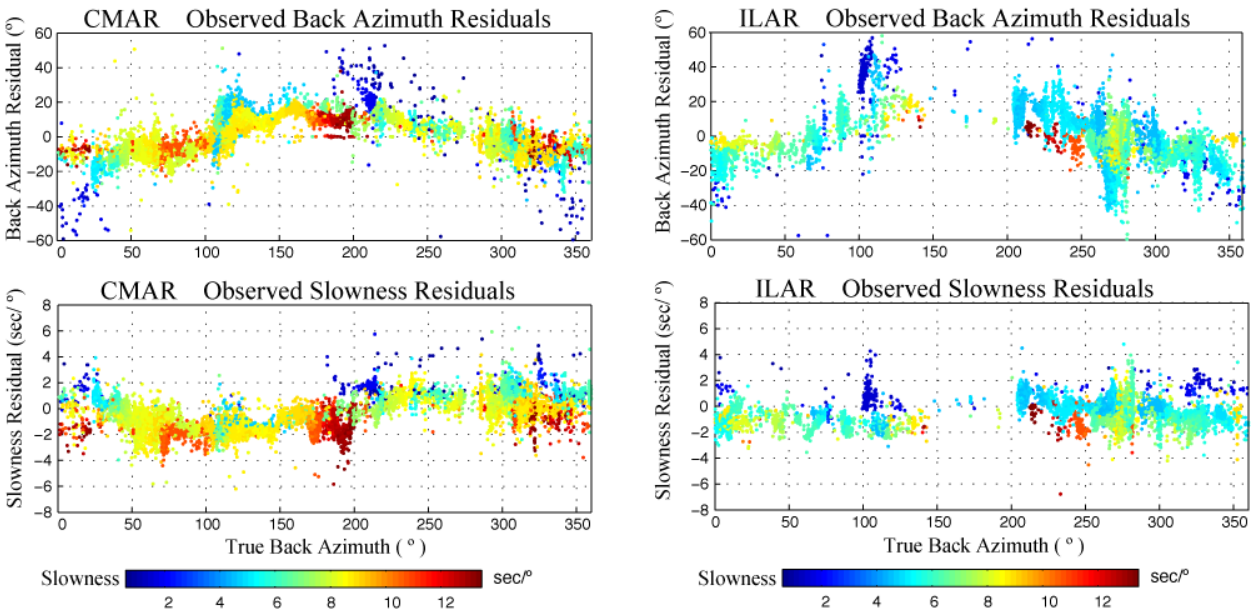

Figure 2. Back azimuth and slowness residuals plotted against true back azimuth for stations CMAR (left) and ILAR (right). Color indicates theoretical slowness of the incident wavefront (in sec/°) based on the iasp91 velocity model and essentially represents the epicentral range. The sinuous trend of the residuals and the affect of slowness on the azimuth residual are both consistent with a dipping interface beneath the array.

Dipping Layer Determination

Niazi (1966) attributed systematic back azimuth and slowness deviations to dipping geologic interfaces under the array, and he derived equations to compute these deviations for a dipping interface. Both back azimuth and slowness residuals have an *asymmetric* cosine shape and their values should be close to zero for rays coming along strike and maximum (absolute value) for rays coming up- or down-dip. This is indicated by the 360° periodicity and 90° phase shift between slowness and back azimuth anomalies (Figure 2). The extent of the azimuth bias varies with the angle of incidence, dip of the Moho, and velocity ratio. The pattern of azimuth perturbation can constrain the dip if the velocity contrast is known, or vice versa, but the pattern is not unique when both dip angle and velocity contrast are varied. Typically one determines the strike from a cosine fit to azimuth residuals then uses that strike to find the dip angle from a cosine fit to the slowness residuals.

The strike is found from the crossover points of the back azimuth residuals and the dip is found from the amplitude of the slowness residuals. The strike of the dipping Moho is the point with the largest azimuth residual following the first zero crossing of the cosine fitting curve. According to Niazi (1966), if the azimuths are read clockwise the direction of the dip is given by the point of transition of the back azimuth residuals from negative to positive values. Both Tibuleac and Stroujkova (2009) and Lindquist *et al*. (2007) used this approach to determine the Moho orientation beneath CMAR and ILAR respectively.

As the refraction of the seismic wavefront follows Snell's law, the effect of a dipping interface on an incident seismic ray may be more directly computed using vector arithmetic and Snell's law (*http://en.wikipedia.org/wiki/Snell's_law*) allowing us to solve for the Moho strike ϕ and dip δ angles by simultaneously fitting both the back azimuth and slowness residuals using:

$$v = \left(\frac{V_2}{V_1}\right) l + \left(\frac{V_2}{V_1}\ COS\Theta_1 + COS\Theta_2\right) n \qquad [1]$$

and

$$COS\Theta_1 = n \cdot (l) \quad , \quad COS\Theta_2 = \sqrt{1 - \left(\frac{V_2}{V_1}\right)^2 (1 - COS^2\Theta_1)}$$

where *l* is the directional vector of the incident ray (determined by theoretical back azimuth and slowness), *v* is the directional vector of the refracted ray, *n* is the normal vector to the dipping-Moho plane (using ϕ and δ), θ_1= angle of incidence, and θ_2= angle of refraction. We use the **iasp91** *P*-wave velocities below and above the Moho, 8.04 and 6.2 km/sec respectively, for v_1 and v_2.

We have written a MATLAB™ code based on equation [1] to invert back azimuth and slowness residual data for the strike and dip of an interface using a multi-variable optimization technique. The forward model may be written in the generalized form:

$$(\Delta\alpha_i, \Delta\mu_i) = f(\phi, \delta, \alpha_i, \mu_i, v_1, v_2) \qquad [2]$$

Where $\Delta\alpha_i$ and $\Delta\mu_i$ are differential back azimuth and slowness residuals for the i^{th} data point (*i.e*., the measured data). The function *f* describes how an incoming plane wave with an expected back azimuth of $\alpha_i$and slowness μ_i, based on the known source receiver configuration, interacts with an oriented plane with specified velocities above and below the boundary (v_1 and v_2 respectively). The goal is therefore to find the optimal orientation of the plane that satisfies equation [2] (*i.e.*, to determine ϕ and δ).

We chose to utilize a pre-existing algorithm from the MATLAB Optimization Toolbox™ called *lsqcurvefit* which is a nonlinear curve-fitting routing that is designed to solve multivariant systems in a least squares sense. In our specific case, the *lsqcurvefit* algorithm searches for the strike and dip of the plane by minimizing:

$$\sum_{i=1}^{n} \{f(\phi, \delta, \alpha_i, \mu_i, v_1, v_2) - (\Delta\alpha_i, \Delta\mu_i)\}^2 \qquad [3]$$

where the summation is over all *n* slowness/azimuth residual data points. The MATLAB™ function utilizes the *trust-region-reflective optimization* algorithm, based on the interior-reflective Newton method developed in Coleman and Li (1994, 1996), to simultaneously search for the optimal strike and dip of the proposed orientation of a plane defining the Moho.

Results

We applied this optimization technique to determine the best-fitting strike and dip of a Moho interface beneath the CMAR array and compare the results using the same data set with Niazi's technique. The azimuth residuals for 9903 *P* phases recorded at CMAR are shown in Figure 3 (top, left) and are fit by an asymmetric cosine curve of the form 1.04 - 14.2*cos(Z − 188.4°) where Z is the true back azimuth computed from **iasp91**. The curve fit is done using the *fminsearch* function in MATLAB™, and as described by Niazi (1966) strike of the dipping Moho is the point with the largest azimuth residual following the first zero crossing of the cosine fitting curve, which in this case is 188.4°. The lower left plot in Figure 3 shows the azimuth residuals distribution after the cosine function has been removed.

Using our optimization method we find that the best fitting Moho at CMAR has strike 192.6° and dip 18.3°. The predicted azimuth residuals from this Moho model are shown in Figure 3 (top, right), and when these values are removed from the observed values the resulting distribution is shown in Figure 3 (lower, right). The major sinuous trend in the residuals is removed, and the correlation between error and theoretical slowness is also mitigated. This shows the importance of using a dipping interface model, which simultaneously fits azimuth and slowness data, in contrast to simply fitting the azimuth trend with a sinusoid. First, a simple sinusoidal curve fit does not account for the strong dependence on slowness. Second, the effect of a dipping interface is not a pure sinusoid. The deviation from a sinusoid becomes stronger as dip angle and slowness increase.

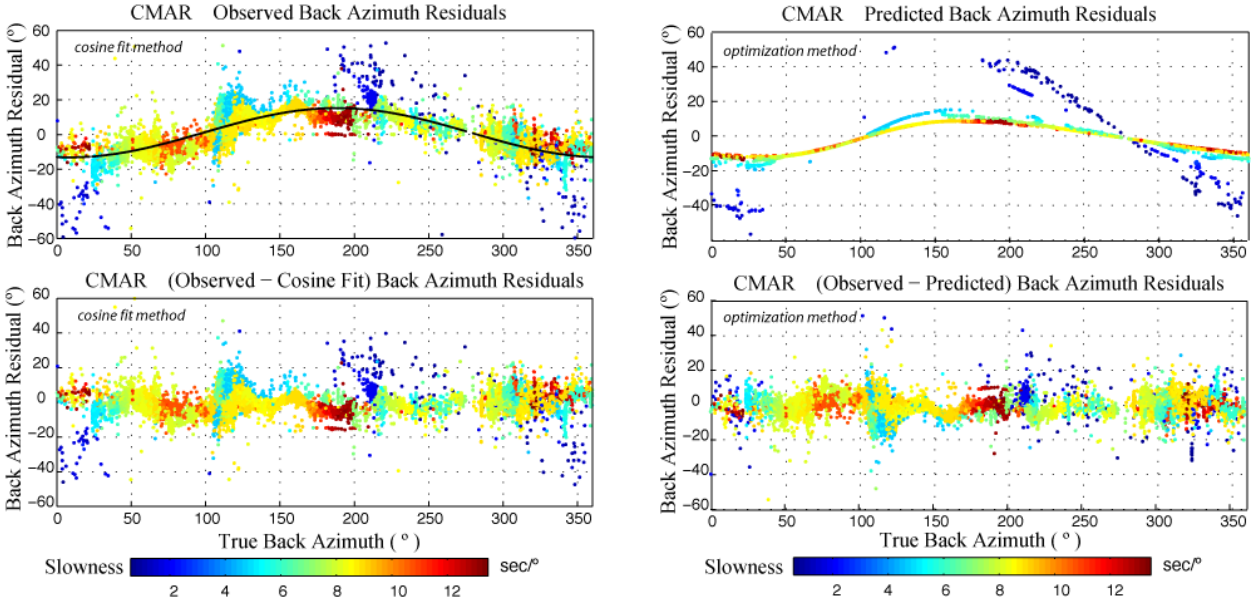

Figure 3. Corrected azimuth residuals at CMAR using the two methods. (Left, top) Azimuth residuals at CMAR with the cosine fit shown by the black line which has the form 1.04 – 14.2* cos(Z- 188.4) and yields a Moho strike estimate of 188.4°. The fit is then subtracted from the residuals to give the corrected distribution (Left, bottom). (Right, top) Azimuth residuals predicted for CMAR from a dipping Moho model, with strike 192.6° and dip 18.3°, obtained from our optimization code which inverts both the azimuth and slowness data for CMAR in Figure 2 simultaneously. (Right, bottom) Azimuth residuals after fitting a dipping interface; both the sinuous trend and variations with predicted slowness are mitigated. See Table 1 for goodness of fit statistics.

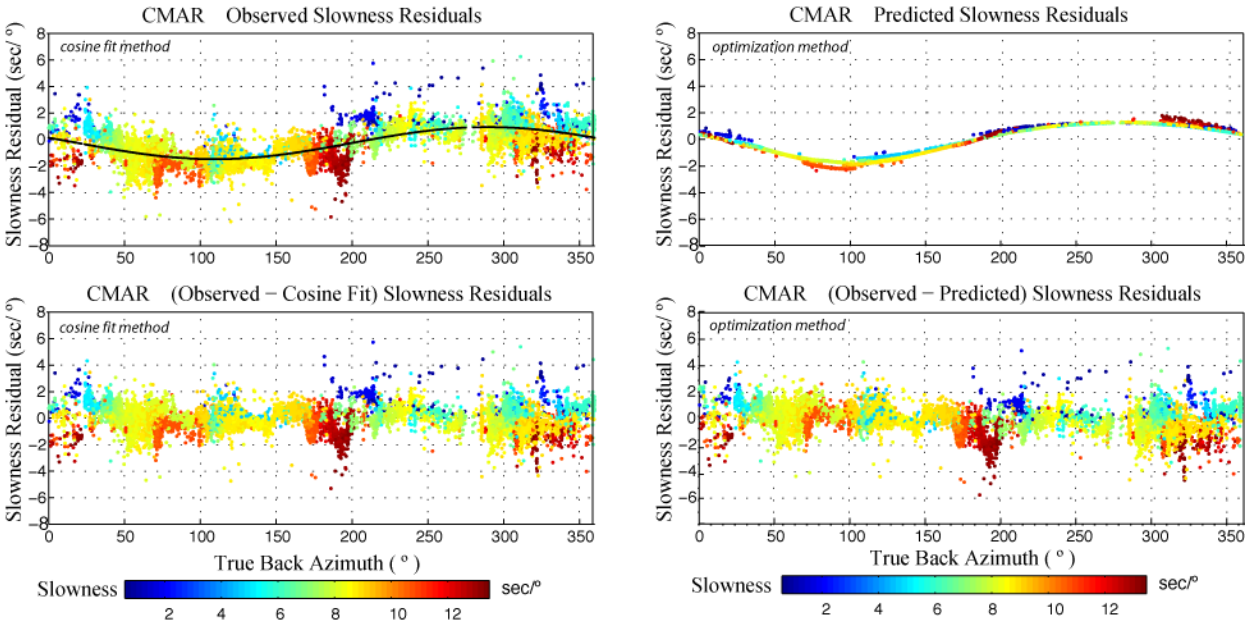

Figure 4. Corrected slowness residuals at CMAR using the two methods. (Left, top) Slowness residuals for CMAR with the cosine fit shown by the black line which has the form 0.27 + 1.2*cos(Z+70.4) and yields a Moho dip estimate of dip 13.1° or 16.8°. The fit is then subtracted from the residuals to give the corrected distribution (Left, bottom). (Right, top) Slowness residuals predicted for CMAR from a dipping Moho model, with strike 192.6° and dip 18.3°, obtained from our optimization. (Right, bottom) Slowness residuals after fitting a dipping interface; both the sinuous trend and variations with predicted slowness are mitigated. See Table 2 for goodness of fit statistics.

Slowness residuals for CMAR are shown in Figure 4 (top,left). Slowness is not as strongly affected by incoming ray angle as azimuth for the CMAR case, but the change in slowness can become strongly dependent on incident angle if the interface dips steeply. Using the Niazi method, the Moho dip is found by forward prediction using the strike=188.4° and the median incident angle (determined from the median slowness) for this data set. We find a Moho dip of 13.1° or 16.8° depending on whether we minimize the fit to the azimuth residuals or the slowness residuals respectively. Since this method does not account for the effects of varying incidence angle (or slowness), it cannot provide corrections for the full suite of observed azimuths and slownesses as they are coupled. . Our optimization method shows significant variance and SMAD reduction (SMADR) over the Niazi method for both azimuth and slowness although it is particularly good for azimuth as one may expect due to the strong dependency on incident angle (see Table 1 and Table 2).

The predicted slowness residuals obtained from our optimization code are shown in Figure 4 (top, right), and the slowness residuals after removing the predicted values are shown in Figure 4 (bottom, right) . There is a dependence of the slowness residual on theoretical slowness (incoming ray inclination), but this effect is not as great as the effect on azimuth residual (Figure 3). This observation is reflected in the statistics listed in Table 1 and Table 2 where the SMAR values show our optimization method is significantly better for azimuth and moderately better for slowness.

Tibuleac and Stroujkova (2009) also estimated the parameters of a dipping Moho under CMAR (strike=197.7° or 213.5° and dip=18.4° or 15.5° using the forward-modeling method of Niazi; the results are for two different methods) using the forward-modeling method of Niazi (1966). Our resulting Moho strike and dip estimates are in very good agreement with these previously published values.

Table 1. Summary Statistics for Azimuth Residuals at CMAR

	Observed	Cosine fit Corrected	Optimization Corrected
Mean (°)	0.988	0.987	-0.745
Median (°)	0.649	2.720	-0.842
rms (°)	0.102	0.082	0.062
SMAD (°)	12.795	12.46	4.924
Variance (°)	121.38	78.92	44.82
SMADR		2.57%	61.51%
Variance Reduction		34.98%	63.07%

Table 2. Summary Statistics for Slowness Residuals at CMAR

	Observed	Cosine fit Corrected	Optimization Corrected
Mean (sec/°)	-0.492	-0.492	0.100
Median (sec/°)	-0.646	-0.801	-0.016
rms (sec/°)	0.012	0.009	0.008
SMAD (sec/°)	1.406	0.991	0.692
Variance(sec/°	1.618	0.876	0.813
SMADR		29.49%	50.82%
Variance Reduction		45.84%	49.74%

CONCLUSIONS AND RECOMMENDATIONS

We have developed a new method for modeling the strike and dip of the Moho beneath a seismic array by simultaneously fitting the sinusoidal pattern of azimuth and slowness deviations from a one-dimensional velocity model. The new method is tested at CMAR for over 9900 observations, and we determine the Moho beneath this array to have a strike angle of 192.6° and a dip angle of 18.3° which are in good agreement with previous estimates made by Tibuleac and Stroujkova (2009). When the dipping Moho predictions are removed from the azimuth and slowness residuals, both the sinuous trend and variations with predicted slowness are mitigated. While a single dipping interface model does not account for all of the discrepancy between observed and predicted back azimuth and slowness anomalies, this technique is a good first step in the calibration procedure for arrays exhibiting sinusoidal residual trends. Additional modeling with multiple dipping interfaces included within the outlined optimization scheme should be pursued.

ACKNOWLEDGEMENTS

Thank Ileana for helpful discussions and making available her MATLAB™ script to fit the Moho dip angle using the Niazi method. We are also grateful to Stan Ruppert for helpful comments on this paper. This work was performed under the auspices of the U.S. Department of Energy Lawrence Livermore National Laboratory, *Contribution LLNL-CONF-563592*.

REFERENCES

Bondar, I., R. G. North, and G. Beall (1999). Teleseismic slowness-azimuth station corrections for the International Monitoring System Network, *Bull. Seism. Soc. Am.* **89,** 989–1003.

Capon, J. (1969). High-resolution frequency-wavenumber spectrum analysis, *Proc. IEEE* **57,** 1408–1418.

Coleman, T.F. and Y. Li, (1994). On the Convergence of Reflective Newton Methods for Large-Scale Nonlinear Minimization Subject to Bounds, *Mathematical Programming*, **67** (2), 189-224, 1994.

Coleman, T.F. and Y. Li, (1996). An Interior, Trust Region Approach for Nonlinear Minimization Subject to Bounds, *SIAM Journal on Optimization,* **6**, 418-445.

Greenfield, R. J. and R. M. Sheppard (1969). The Moho depth variations under the LASA and their effect on $dT/d\Delta$ measurements, *Bull. Seis. Soc.Am.,* **59**, 409-420.

Havskov, J. and E. R. Kanesewich (1978). Determination of the dip and strike of the Moho from array analysis, *Bull. Seis. Soc.Am.,* **68**, 1415-1419.

Kennett, B.L.N. and E.R. Engdahl (1991). Traveltimes for global earthquake reference location and phase identification, *Geophys. J. Int,* **105**, 429-465.

Koch, K. and U. Kradolfer (1997). Investigation of azimuth residuals observed at stations of the GSETT-3 alpha network, *Bull.Seism.Soc.Am.,* **87,** 1576–1597.

Kvaerna, T. and D. J. Doornbos (1986), "An Integrated Approach to Slowness Analysis With Arrays and Three-component Stations", Semiannual Technical Summary, 1 October 1985 - 31 March 1986, NORSAR sci. Rep. 1-86/87, Kjeller Norway.

Lin, C-H. and S. W. Roecker (1996). *P*-wave back azimuth anomalies observed by a small-aperture seismic array at Pinyon Flat, Southern California: Implications for structure and source location, *Bull.Seism.Soc.Am.,* **86,** 470-476.

Lindquist, K. G., I. M. Tibuleac, and R. A. Hansen (2007). A semiautomatic calibration method applied to a small-aperture Alaskan seismic array, *Bull.Seism.Soc.Am.,* **97,** 100-113, doi: 10.1785/0120040119.

Menke, W. and V. Levin (2002). Anomalous seaward dip of the lithosphere-asthenosphere boundary beneath northeastern USA detected using differential-array measurements of Rayleigh waves, *Geophys. J. Int.*, **149**, 413-421.

Niazi, M. (1966). Corrections to apparent azimuths and travel-time residuals for a dipping Mohorovicic discontinuity, *Bull.Seism.Soc.Am.,* **56,** 491–509.

Otsuka, M. (1966a). Azimuth and slowness anomalies of seismic waves measured on the Central California Seismographic Array, part I: Observations, *Bull.Seism.Soc.Am.,* **56,** 223–239.

Otsuka, M. (1966b). Azimuth and slowness anomalies of seismic waves measured on the Central California seismographic array, Part II: Interpretation, *Bull.Seism.Soc.Am.,* **56,** 655–675.

Ram, A. and L. Yadav (1984). Structural corrections for slowness and azimuth of seismic signals arriving at Gauribidanur array, *Bull.Seism.Soc.Am.,* **74,** 97-105.

Rhodes, B. P., R. Conejo, T. Benchawan, S. Titus, and R. Lawson (2005). Paleocurrents and provenance of the Mac rim formation, Northern Thailand: Implications for tectonic evolution of the Chiang Mai Basin, *J. Geological Soc*., **162** (1), 51-63; doi: 10.1144/0016-764903-128.

Ringdal, F. and E. S. Husebye (1982). Application of arrays in detection, location and identification of seismic events, *Bull.Seism.Soc.Am.,* **72,** S201–S224.

Rost, S. and C. Thomas (2002). Array seismology: methods and applications, *Rev.Geophys.,* **40,** 2-1 – 2-27.

Schweitzer, J. (2001). Slowness Corrections – One way to improve IDC products, *Pure Appl. Geophys.*, **158**, 375-396.

Tibuleac, I. M. and E. T. Herrin (1997). Calibration studies at TXAR, *Seism.Res.Lett.,* **68,** 353–365.

Tibuleac, I. M. and E. T. Herrin (2001). Detection and location capability at NVAR for events on the Nevada Test Site, *Seism.Res.Lett.,***72,** 97–107.

Tibuleac, I. M. and A. Stroujkova (2009). Calibrating the Chiang Mai seismic array (CMAR) for improved event location, *Seism.Res.Lett,* **80,** 579-590, doi: 10-1785/gssrl.80.4.579.

Zengeni, T. G. (1970). A note on an azimuthal correction for $dT/d\Delta$ for a single dipping plane interface, *Bull.Seism.Soc.Am.,* **60,** 299-306.